RSC Advances

ROYAL SOCIETY OF CHEMISTRY

www.rsc.org/advances

A novel biosensor for silver(I) ion detection based on nanoporous gold and duplex–like DNA scaffolds with anionic intercalator

Yaoyu Zhou [ab], Lin Tang [*ab], Guangming Zeng [*ab], Jingjing Zhu [ab], Haoran Dong [ab], Yi Zhang [ab], Xia Xie [ab], Jiajia Wang [ab], Yaocheng Deng [ab]

a College of Environmental Science and Engineering, Hunan University, Changsha, 410082, China,

b Key Laboratory of Environmental Biology and Pollution Control (Hunan University), Ministry of Education, Changsha 410082, Hunan, PR China.

[*] Corresponding author: Tel.: +86–731–88822778; Fax.: +86–731–88822778

E–mail: tanglin@hnu.edu.cn(L. Tang), zgming@hnu.edu.cn (G.M. Zeng).

Abstract

This study demonstrates a novel biosensor for silver(I) ion detection based on nanoporous gold (NPG) and duplex–like DNA scaffolds with anionic intercalator. The hairpin structure was formed initially through hybridization with the unlabeled probe (S1+S2+S3). In the presence of Ag^+, the structure of immobilized DNA changed to duplex–like structure, and formed a C–Ag^+–C complex at electrode surface. The response current of the modified electrode after immersing in the disodium anthraquinone–2,6–dissulfonate (AQDS) as the signal agent was changed. And an increased current was obtained, corresponding to Ag^+ concentration. NPG provided faster electron transfer and an excellent platform for DNA immobilization. Under optimal conditions, silver(I) ion could be detected in the range from 1×10^{-10} M to 1×10^{-6} M, and the lower detection limit of the biosensor for Ag^+ is 4.8×10^{-11} M with good specificity. The results showed that this novel approach provided a reliable method for the quantification of Ag^+ with sensitivity and specificity, which was potential for practical applications.

Introduction

As we all know, even at a trace level, toxic metals entering the environment by industrial activities act as severe environmental pollutants and pose serious risk to human health due to the non–biodegradability and accumulation in the food chain[1-4]. Therefore, heavy metal pollution received considerable attention for global sustainability. Recently, silver ions (Ag^+) have received a major concern among these toxic metal ions, which might be ascribed to that silver is widely used in photography and imaging industry, pharmacy and the electrical industry. What's more, recent studies emphasized the potential negative impact and bioaccumulation of Ag^+ on aquatic organisms[5,6]. For example, environmentally benign bacteria will die when exposed in water with a dose of Ag^+ for a long term[5]. Na^+ and Cl^- homeostasis of invertebrates and fishes will perturb even exposed in nanomolar concentration of Ag^+ ion[7]. It is therefore essential to monitor Ag^+ in the natural water environment worldwide. Conventional quantitative methods, such as inductively coupled plasma mass spectrometry (ICP–MS)[8], electrothermal atomic absorption spectrometry (ETAAS)[9], and etc., have been extensively applied to quantify Ag^+ with high selectivity and sensitivity. In addition to the tedious sample preparation and expensive and complex instrumentations, these methods normally involve sophisticated pre–concentration procedures for extracting metal ions from samples, in which the speciation change of metal ions is unavoidable[10].

It is known that DNA can interact with some types of metal ions to form stable metal–mediated DNA duplexes with high specificity[11,12]. For example, Hg^{2+} can specifically interact with thymine–thymine (T–T) mismatch to form stable T–Hg^{2+}–T complexes[11,13]. For lead ions (Pb^{2+}) detection is based on the Pb^{2+}–stabilized G–quadruplex and the Pb^{2+}–dependent DNAzyme[14]. Therefore, many efforts have been focused on the design of DNA–based biosensors to detect Pb^{2+} and Hg^{2+}. As for Ag^+, since Ono and co–works found that Ag^+ ions could specifically interact with the cytosine–

cytosine (C–C) mismatch in DNA duplexes to form stable C–Ag^+–C complexes[15], various C–Ag^+–C based biosensors have been developed with good selectivity and high sensitivity[16-18]. Besides, DNA biosensors based on hairpin structure have received a major concern, because this structure sensors have higher detection stability and sensitivity compared to linear DNA structures sensors[19,20]. Moreover, this kind of sensors is generally specific to a given target owing to their highly constrained conformations, and mostly insensitive to other interferents even in complex environments, which may improve the potential application in real environment[21].

However, a high electron transfer and effective immobilization platform for the DNA scaffold is also a key issue in the detection system[1]. In recent years, various nanomaterials were employed as DNA immobilization substrates and recognition elements in biosensors. For example, Mulchandani and co–workers reported a selective and sensitive biosensor for the detection of Hg^{2+} based on single–walled carbon nanotubes (SWCNTs)[22]. Zhang and co–workers developed a sensitive chronocoulometric biosensor for DNA detection using gold nanoparticles/multi–walled carbon nanotubes[23]. In our previous study, we used ordered mesoporous carbon nitride (MCN) and ordered mesoporous carbon (OMC) as the platform for electrochemical biosensors[24-26]. These biosensors could increase the sensitivity and lower the detection limit, and improve the possibility of the application for portable devices for real–time and on–site detection. In this study, nanoporous gold (NPG) was used as sensing interface to immobilize the DNA. In addition to its higher conductivity, excellent structural continuity and general biocompatibility[27-30], NPG also provides a natural platform for stable DNA immobilization because of the strong gold–sulfur (Au–S) covalent–type interactions, which might extend the using life and stability of the biosensor, and make the sensor assembly process easier. Though gold nanoclusters have been used in biosensors[31,32], little attention has been paid to silver ion sensors based on Ag^+–specic oligonucleotides. Besides, the choice of

signal indicator is also of great significance for the construction of a DNA sensor. Previous studies have demonstrated that the bindings of disodium–anthraquinone–2,6–disulfonate (AQDS) to DNA are completely through electrostatic interaction for mercuric ions detection with high sensitivity[33]. AQDS exhibits a reversible 2–electron transfer process for its quinone/hydroquinone redox couple in electrochemistry containing a perfectly symmetric anthraquinone ring structure. Therefore, AQDS, an anionic intercalator, was used for the proposed biosensor.

Herein, Ag^+–specic oligonucleotides, nanoporous gold (NPG), and disodium–anthraquinone–2,6–disulfonate (AQDS) were used to construct a highly sensitive sensor for silver ions detection in environmental samples. This strategy for Ag^+ quantification is highly accurate, relatively simple to operate, and to exploit strong resistance of the sensor to environmental impact disturbance. The NPG were electrodeposited on a glassy carbon electrode surface, and then modified with mercury Ag^+–specic oligonucleotide probes. In the presence of Ag^+, the probes form a hairpin structure because of C–Ag^+–C mismatches. Meanwhile, AQDS was selected as an electroactive signal indicator because of its good electrochemical performance. Furthermore, Ag^+ detection in environmental samples was performed to investigate and demonstrate the application of the proposed biosensor.

Experimental

Reagents and apparatus

Disodium–anthraquinone–2,6–disulfonate was purchased from Tokyo Chemical Industry Co., Ltd. (Tokyo, Japan). Tris (2–carboxyethyl)phosphinehydrochloride (TCEP), tris (hydroxymethyl) aminomethane and 6–mercaptohexanol (MCH) were purchased from Sigma–Aldrich (USA). $AgNO_3$, HNO_3, $K_3Fe(CN)_6$, $K_4Fe(CN)_6$, and all other chemicals were of analytical grade and used as received. All aqueous solutions were prepared with ultra–pure water (18 MΩ·cm, Milli–Q,

Millipore). 25 mM tris–acetate buffer (pH 7.4) containing 300 mM $NaClO_4$ and phosphate buffer saline (PBS, 0.1 M KH_2PO_4 and 0.1 M Na_2HPO_4) were used in this work.

The synthesized oligonucleotides used for hybridization in our experiment, all HPLC–puried and lyophilized, were provided by Sangon Biotech (Shanghai, China). The sequences were as follows:

5'–HS–$(CH_2)_6$–SS–$(CH2)_6$–TCA–GAC–TAGC–CCC–CCC–CCC–CCC–GG–ACG–3' (S1)

5'–CC–TGC–TTT–CGT–CC–3' (S2)

3' –AGT–CTG–ATCG–CCC–CCC–CCC–CCC–GG–ACG–5' (S3)

Probes were dissolved in Tris–ClO_4 buffer (pH=7.4) containing 300 mM $NaClO_4$ and kept at –20 ˚C for further use. PBS (pH 7.0) containing 0.2 M NaCl was used to store the 1 mM AQDS, in the dark.

All electrochemical measurements, such as cyclic voltammograms (CVs), electrochemical impedance spectroscopy (EIS) and square wave voltammetry (SWV), were performed in a conventional three–electrode cell at room temperature with a CHI760D electrochemical workstation (Chenhua Instrument Shanghai Co., Ltd., China). Field emission SEM (JSM. ihangh was used to gained scanning electron microscope (SEM) image. A model pHSJ–3 digital acidimeter (Shanghai Leici Factory, China) was used to measure the solution pH. A Sigma 4K15 laboratory centrifuge, a vacuum freezing dryer and a mechanical vibrator were used in the assay.

Sensor fabrication

The nanoporous gold (NPG) foil was prepared by selective dissolution of Ag from Ag/Au according to the report [27,31,32]. The alloy was corroded in concentrated HNO_3 at 25 ˚C, and the NPG was then thoroughly washed to the neutral pH with ultrapure water. The bare glass carbon electrode (GCE) was polished in alumina slurry firstly, and then rinsed with deionized water. Afterwards the electrode was etched for about 10 min in a "Piranha" solution (98% H_2SO_4 : 30% H_2O_2 3 : 1(v/v)) to

remove organic contaminants (*Caution: Piranha solution reacts violently with organic materials, thus should be handled with extreme care)*[24,25]. Finally, the electrode surface was treated by H_2SO_4 (0.5 M) with cyclic voltammetry scan (between 0 and 1.2 V at the scan rate of 50 mV s^{-1}) until a reproducible scan was obtained. After being dried, the nanoporous gold was carefully coated onto a pretreated GCE via physical adsorption after being washed with ultrapure water to neutralize the NPG foil (prepared by selective dissolution of Ag from Ag/Au).

Subsequently, the mixture solution (2 μL S1, 25 mM tris–acetate buffer (pH 7.4), and 1 mM TCEP (which is included to reduce disulfide bonded oligomers) was dropped onto the electrode surface for self–assembling through Au–S bonding for 10 h in 4 ˚C. The probes of this biosensor were hybridized as follows. 6–mercapto–1–hexanol (MCH) solution (400 μL) was used to immerse the modified electrode with S1 probes with 1h to improve the stability and quality, to reduce nonspecific adsorption of DNA and to obtain a well aligned DNA monolayer[34]. After that, the modified electrode was soaked in the 2.5 μM DNA solution containing S2 and S3 (1:1), which is to form the hairpin structure (S1+S2+S3) with the incubated time of 1 h in 4 ˚C. Finally, it was washed with tris–acetate buffer (pH=7.4). The electrode was stored in a moist state at 4 ˚C when not in use.

Detection process

Firstly, the modified electrode was treated with various concentrations of Ag^+ in buffers (25 mM tris–acetate, 0.3 M NaCl, pH 7.4) for 2 h. Subsequently, it was washed with tris–acetate buffer (pH=7.4). A conventional three–electrode system was used. Electrochemical impedance spectroscopy (EIS), cyclic voltammograms (CVs) were performed in 0.1 M PBS (pH 7.4) containing 10 mM KCl and 5 mM $Fe(CN)_6^{3-/4-}$ (1:1). Besides, square wave voltammetry (SWV) measurements were performed from –620 to –5 mV under a pulse amplitude of 25 mV and a frequency of 10 Hz, with a step potential of 4 mV. And all the measurements were carried out at room temperature.

Results and discussion

Design of biosensing strategy

Fig. 1 illustrates the preparation processes of the duplex–like DNA scaffolds biosensor, and may outline the principle of the proposed method for the highly sensitive quantification of Ag^+ ions. Here, in order to achieve the automatic formation of duplex–like DNA scaffolds structure, three auxiliary DNA probes, named S1, S2 and S3, are ingeniously designed. This strategy involves the self–assembly of S1 at glassy carbon electrodes modified with NPG via Au–S bonding[33,35,36]. Subsequently, the hairpin structure will be automatically formed after the MCN and mixed solution (S2+S3) are added in the sensing system respectively. In the presence of Ag^+, the probes form a duplex–like DNA scaffolds structure. Meanwhile, AQDS was used as an electroactive signal indicator. Besides, it is important to control the quality of self–assembled monolayers of DNA (S1) at the modified electrode surfaces. As we known, thiolated DNA strands stay in a conformation that is nearly perpendicular to surfaces, however, there might exist multiple contacts at gold surfaces[37]. We have previously demonstrated that MCH displaces weakly bound DNA strands from the surface, forms a dense sublayer that detaches the backbones of the linked DNA strands from the surface, and helps DNA "stand up" on gold surface[34]. In addition, the density of the probe also affects the hybridization efficiency significantly, and thus enhances or reduces the performance of biosensor. Previous studies also demonstrated that precise control of DNA assembly at electrode surfaces can be achieved by optimizing time course for self–assembly and probe concentration[33]

"**Here Fig. 1**"

As seen in Fig. 2, the anodic peak potential of AQDS was nearby –0.45 V at the electrode, which was similar with our previous work [32]. Fig. 2 displays the SWV curves with biosensor in the presence and absence of Ag^+ ions. After addition of Ag^+ (10^{-6} M), the hairpin structure underwent a

conformational alteration through the Ag(I)–mediated formation of C–Ag^+–C base pairs (Fig. 1), which resulted in the quantity increase of AQDS attached on the electrode surface, leading to the increase of the electrochemical signal. Besides, the metal ion–mediated C–Ag^+–C formed DNA duplex–like scaffolds enhanced the electron transfer[33,38]. In fact, the changes of SWV signal in the presence and absence of the metal ion were different and dependent on the concentration of the given metal ion. On the basis of the results discussed above, the interactions between DNA and Ag^+ led to the increased SWV signal, which was used for the detection of Ag^+.

"**Here Fig. 2**"

Characterization of NPG and electrode assembly process

The SEM image of NPG in Fig. 3A illustrates an open three–dimensional nanoporous structure, which suggests that NPG film has been deposited on the GCE surface successfully. Besides, to test the performance of the modified electrode, CV was carried out in phosphate buffer (containing 5 mM $Fe(CN)_6^{3-/4-}$ (1:1) and 10 mM KCl, pH 7.4). As seen in Fig. 3B, the peak current of the redox probe was increased significantly after the immobilization of NPG on the GCE. These cyclic voltammograms also proved that the electrode had a good current response capability. Correspondingly, EIS showed that the impedance of the NPG/GCE and bare GCE in phosphate buffer. An almost straight line was observed with NPG assembled, and the value of R_{CT} was calculated to be 19.9 Ω (Table S1) according to the reported method in our lab[39,40]. An obvious increase in the interfacial resistance was observed from the GCE (Fig. 2B), and the value of R_{CT} was increased to 760.0 Ω (Table S1), which indicated that the introduction of NPG could enhance the electron transfer kinetics to a large extent. What's more, the electron transfer ability of the modified electrode reflected by EIS was in accordance with the current density response reflected by CV.

"**Here Fig. 3**"

Optimization of the variables of experimental conditions

A series of experiments was performed to optimize the experimental conditions before the quantitative analysis of Ag^+ to obtain acceptable signal response. The capture probe (S1) was self–assembled on the modified electrode surface for 2, 4, 6, 8, 10 and 12 h. As shown in Fig. S–1A, the most efficient result was obtained when 2 uM of S1 self–assembled for 10 h in the subsequent measurements. Similarly, the optimization of hybridization time of DNA hybridization (S2+S3) with S1 reaction was revealed. When the time increased from 30 to 60 min, the response current increased because of more and more probes (S2+S3) hybridizing with S1 in this process, and then leveled off for the hybridization of amount of (S2+S3) with S1 became saturated (As seen in Fig. S–1B). In order to obtain the maximum loading of Ag^+ on the sensor interface, the time–course of the Ag^+ complexing with C bases was studied (As shown in Fig. S–1C). The experimental data indicated that the adsorption quantity of Ag^+ relied much on the time accretion. With the incubation time increasing, the charge was enlarged. After about 120 min, it kept constant at a saturation value, indicating that the incubation time of 120 min was efficient which was used in all subsequent analyses. Besides, as we known, there is a certain resistance from electrostatic repulsion when AQDS is intercalated into duplexlectrostatic repulsiontion time biosensor. Therefore, the intercalation process of AQDS is relatively slow. But suitably high salt concentration can speed up the intercalation by screening the electrostatic repulsion between the two. When the sensor was immersed in AQDS solution containing 0.2 M of NaCl for 360 minutes, the current response reached a maximum (As shown in Fig. S–1D).

Response of the sensor to Ag^+ concentration

Under the optimum conditions, the square wave voltammetry (SWV) was used to record the current of various Ag^+ concentrations with the biosensor, and the results are shown in Fig. 4. From

this figure, it can be observed that the current of AQDS increases with increases of the concentration of Ag^+. Besides, it is linear with the logarithm of the concentration of the complementary Ag^+ from 10^{-10} to 1.0^{-6} M. The linear regression equation was $Y = (4.2240\pm0.0375)X + (-0.1920\pm0.0046)$ (Y is the current (uA), X is the common logarithmic value of the target concentration (M)) with a correlation coefficient R^2=0.9983. The detection limit of the biosensor was estimated to be 4.8×10^{-11} M, based on signal/noise ratio = 3. This biosensor exhibited improved analytical performances in terms of linear detection range, and showed lower detection limit. The limit of detection was competitive with other highly sensitive detection approaches such as fluorescence, colorimetry and electrochemical methods, as presented in Table 1.

"**Here Fig. 4**"

"**Here Table 1**"

The stability, repeatability, reproducibility and selectivity of the biosensor

As a DNA sensor, the repeatability is an important factor to be considered. In this work, we examined the repeatability of the same biosensor by detecting 1×10^{-8} M Ag^+ (As shown in Fig. 5). The relative standard deviation (R.S.D.) value was 4.1% with three determinations, which implied the measurements had good repeatability with no need to apply a complicated pretreatment procedure to the electrode.

"**Here Fig. 5**"

The reproducibility of this biosensor was investigated. Five biosensors were fabricated with five different GCEs by the same steps independently, and used to detect 1×10^{-8} M Ag^+, as presented in Fig. S–2A. The RSD was 4.9% with five biosensors prepared independently, indicating that the fabrication procedure was reliable, and this biosensor had good reproducibility.

The stability of the biosensor was also explored. We investigated the stability of this sensor through the response to 1×10^{-8} M Ag^{+} for 1 month (as shown in Fig. S–2B). Beyond this period, the experiment was carried out per 5 days. When not in use, the electrode was stored in a moist state at 4 ˚C. The result showed that the biosensor retained about 81% of its original ΔI after 1 month. The relatively good stability of the biosensor may be explained by the fact that the hairpin structure and the specific recognition ability to form C–Ag^{+}–C could be protected effectively. Besides, the film of NPG could provide a biocompatible microenvironment.

The sensing interfaces were determined with various competing trivalent (or divalent) metal ions which are commonly present in real samples, such as Pb^{2+}, Cr^{3+}, Co^{2+}, Hg^{2+}, Cu^{2+}, Cd^{2+}, to verify the selectivity of this approach for the detection of Ag(I) in practical applications. Under the same experimental conditions, each competing metal ion was tested at 1×10^{-6} M, 1×10^{-5} M, 1×10^{-4} M. As seen in Fig. 6, none of the corresponding ΔI of the tested metal ions was higher than half of that produced by 1×10^{-8} M, 1×10^{-7} M, 1×10^{-6} M Ag^{+}. Such excellent selectivity is attributed to the duplex–like DNA scaffolds structure with specific C–Ag^{+}–C base pairing which relates closely with signal change as mentioned above. The sensor exhibited good anti–interference ability and provided the potential to selectively determine Ag^{+} levels in real samples.

"**Here Fig. 6**"

Real samples detection

As a further step, we attempted to prove the general applicability of this sensor to practical samples. Four water samples were collected from Taozi Lake, Changsha, Hunan Province, and no Ag^{+} can be detected in these samples. After filtered through a 0.2 mM membrane to remove oils and other organic impurities, the samples were spiked with standard solutions of Ag^{+} prior to measurement. As presented in Table S–2, the relative standard deviation of two methods is no more

than 3.37%. However, compared with the limitations of the AAS method in application, tedious pretreatments, greater consumption of reagents, and a large instrument, the current method possessed certain advantages. The results indicated the potential of the sensor as a simple and reliable analysis method of Ag^+ ions in environmental samples.

Conclusion

In conclusion, a biosensor consisting of nanoporous gold (NPG), and duplex–like DNA scaffolds with anionic intercalator was developed, which provided the potential to quantify trace levels of Ag^+ in environmental water samples. NPG, duplex–like DNA scaffolds and the anionic intercalator improved the detection performance of the sensor significantly, and it exhibited satisfactory results for Ag^+ ion detection with high sensitivity and selectivity. This sensor exhibited relatively wide dynamic working ranges (1×10^{-6}–1×10^{-10} M) and detection limits (4.8×10^{-11} M). It has good potential for application in real water monitoring. Furthermore, alternative sensing devices for other metal ions may be developed as well using other natural or synthetic specific hairpin probes.

Supporting Information

More details about the optimization of experimental conditions, the reproducibility and stability of the biosensor, and analysis of Ag^+ in real samples. This material is available free of charge via the Internet at http://pubs.acs.org.

Acknowledgments

The study was financially supported by the National Program for Support of Top–Notch Young Professionals of China (2012), the National Natural Science Foundation of China (51222805), the Program for New Century Excellent Talents in University from the Ministry of Education of China (NCET–11–0129), Interdisciplinary Research Project of Hunan University, the Fundamental Research Funds for the Central Universities, Hunan University.

References

1 G. Xu, G. Wang, Y. Zhu, L. Chen, X. He, L. Wang, X. Zhang, Biosensors and Bioelectronics, 2014, **59**, 269–275.

2 H.L.Li, J.F. Zhai, X.P. Sun, Langmuir, 2011, **27**, 4305–4308.

3 G.M. Zeng, L. Tang, G.L. Shen, G.H. Huang, C.G. Niu, International Journal of Environmental Analytical Chemistry, 2004, **84**, 761–774.

4 C.Y. Lin, C.J. Yu, Y.H. Lin, W.L. Tseng, Analytical Chemistry, 2010, **82**, 6830–6837.

5 M.N. Croteau, S.K. Misra, S.N. Luoma, E. Valsami–Jones, Environmental Science & Technology, 2011, **45**, 6600–6607.

6 V.P. Hiriart–Baer, C. Fortin, D.Y. Lee, P.G.C. Campbell, Aquatic Toxicology, 2006, **78**, 136–148.

7 J.R. Shaw, C.M. Wood, W.J. Birge, C. Hogstrand, Environmental Toxicology and Chemistry, 1998, **17**, 594–600.

8 F. Laborda, J. Jiménez–Lamana, E. Bolea, J.R. Castillo, Journal of Analytical Atomic Spectrometry, 2011, **26**, 1362–1371.

9 T. Shamspur, M.H. Mashhadizadeh, I. Sheikhshoaie, Journal of Analytical Atomic Spectrometry, 2003, **18**, 1407–1410.

10 N. Pourreza, H. Parham, A.R. Kiasat, K. Ghanemi, N. Abdollahi, Talanta, 2009, **78**, 1293–1297.

11 G. Clever, X, H., C. Kaul, T. Carell, Angewandte Chemie International Edition, 2007, **46**, 6226–6236.

12 I. Willner, M. Zayats, Angewandte Chemie International Edition, 2007, **46**, 6408–6418.

13 Y. Tanaka, S. Oda, H. Yamaguchi, Y. Kondo, C. Kojima, A. Ono, Journal of the American Chemical Society, 2006, **129**, 244–245.

14 T. Li, S. Dong, E. Wang, Journal of the American Chemical Society, 2010, **132**, 13156–13157.

15 A.Ono, S.Gao, H.Togashin, M.Tashiro, T.Fujimoto, T.Machinami, S.Oda, Y.Miyake, I.Okamoto. Y.Tanaka, Chemical Communications, 2008, **39**, 4825–4827.

16 Y.H. Lin, W.L. Tseng, Chemical Communications, 2009, **43**, 6619–6621.

17 L. Wang, J. Tian, H. Li, Y. Zhang, X. Sun, Analyst, 2011, **136**, 891–893.

18 Y.Y.Zhou, L.Tang, X.Xie, G.M.Zeng, J.J.Wang, G.D.Yang, C.Zhang, Y.Zhang, J.Chen, Y.C.Deng, Analyst, 2014, **139**, 6529–6535.

19 G.Liu, Y.Wang, V.Gau, J.Zhang, L.H.Wang, S.P.Song, C.H.Fan, Journal of the American Chemical Society, 2008, **130**, 6820–6825.

20 S.Y. Niu, Q.Y. Li, R. Ren, S.S. Zhang, Biosensors and Bioelectronics, 2009, **24**, 2943–2946.

21 C.C.Chang, S. Lin, S.C. Wei, C.Y. Chen, C.W. Lin, Biosensors and Bioelectronics, 2011, **30**, 235–240.

22 G. JL, S. T, B. S, M. A., Applied Physics Letters, 2013, **102**, 013701–013703.

23 X. Dong, X. Lu, K. Zhang, Y. Zhang, Microchimica Acta, 2013, **180**, 101–108.

24 L. Tang, Y.Y. Zhou, G.M. Zeng, Z.Li, Y. Zhang. G.D.Yang, X.X. Lei. M.S.Wu, Analyst, 2013, **138**, 3552–3560.

25 Y. Zhou, L. Tang, G. Zeng, J. Chen, Y. Cai, Y. Zhang, G. Yang, Y. Liu, C. Zhang, W. Tang, Biosensors and Bioelectronics, 2014, **61c**, 519–525.

26 J. X. Liu, W. J. Zhou, J. L. Gong, L. Tang, Y. Zhang, H. Y. Yu, B. Wang, X. M. Xu, G. M. Zeng, Bioresource Technology, 2008, **99**, 8748–8751.

27 Y. Ding, Y. Kim, X, J., J. Erlebacher, Advanced Materials, 2004, **16**, 1897–1900.

28 Y. Ding, Y. Ding, MRS Bulletin, 2009, **34**, 569–576.

29 M.D.Scanlon, K.Salaj-Kosla, S.Belochapkine. D.MacAodha, D.Leech, Y.Ding. E.Magner, Langmuir, 2012, **28**, 2251–2261.

30 X. Zhang, Y. Ding, Catalysis Science & Technology, 2013, **11**, 2862–2868.
31 H. Fan, Z. Guo, L. Gao, Y. Zhang, D. Fan, G. Ji, B. Du, Q. Wei, Biosensors and Bioelectronics, 2015, **64**, 51–56.
32 C. Wu, H. Sun, Y. Li, X. Liu, X. Du, X. Wang, P. Xu, C. Wu, H. Sun, Y. Li, Biosensors and Bioelectronics, 2014, **66c**, 350–355.
33 Y. Zhang, G.M. Zeng, L. Tang, Y.P. Li, Z.M. Chen, G.H. Huang, RSC Advances, 2014, **36**, 18485–18492.
34 L. Tang, G.M.Zeng, G.L.Shen, Y. Li, C. Liu, Z. Li, J. Luo, C. Fan, C. Yang, Biosensors and Bioelectronics, 2009, **24**, 1474–1479.
35 H. Haley D, M. Chad A, Nature Protocol, 2006, **1**, 324–336.
36 A.B.Steel, T.M.Herne, M.J.Tarlow, Analytical chemistry, 1998, **218**, 4670–4677.
37 H. Kimura–Suda, D.Y. Petrovykh, M.J. Tarlov, L.J. Whitman, Journal of the American Chemical Society, 2003, **125**, 9014–9015.
38 S.O. Kelley, E.M. Boon, J.K. Barton, N.M. Jackson, M.G. Hill, Nucleic Acids Research, 1999, **27**, 4830–4837.
39 Y.Y. Zhou, L. Tang, G.M.Zeng, J.Chen, J.J.Wang, C.Fan, G.D.Yang, Y.Zhang, X.Xie. Biosensors and Bioelectronics. 2015. **65**,382–389
40 Y.Y. Zhou, L.Tang, G.M.Zeng, C.Zhang, X.Xie, Y.Y.Liu, J.J.Wang, J.Tang, Y.Zhang, Y.C.Deng, Talanta, 2015, DOI information: 10.1016/j.talanta.2015.06.063.
41 K. Mao, Z. Wu, Y. Chen, X. Zhou, A. Shen, J. Hu, Talanta, 2015, **132**, 658–663.
42 X. Chen, Y.H. Lin, J. Li, L.S. Lin, G.N. Chen, H.H. Yang, Chemical Communications, 2011, **47**, 12116–12118.
43 H.Zheng, X.X.Fan, M.Yan, D.Sun, S.Y.Yang, L.J.Yang, J.D.Li, Y.B.Jiang, Chemical Communications, 2012, 48, 2243–2245.
44 Y.M. Sung, S.P. Wu, Sensors & Actuators B Chemical, 2014, **197**, 172–176.
45 T. Li, L. Shi, E.W.P. Dr., S.D. Prof., Chemistry – A European Journal, 2009, **15**, 3347–3350.
46 Z.Z.Lin, X.H.Li, H.B.Kraatz, Analytical chemistry, 2011, 83, 6896–6901.
47 C. Zhao, K. Qu, Y. Song, C. Xu, J.R. Ren, X.G.Qu, Chemistry A European journal, 2010, 16, 8147–8154.
48 H.C.Yang, X.X.Liu. R.H.Fei, Y.G.Hu. Talanta, 2013, **116**, 548–553.
49 Q. Liu, F. Wang, Y. Qiao, S. Zhang, B. Ye, Electrochimica Acta, 2010, **55**, 1795–1800.
50 J.H. Guo, D.M. Kong, H.X.Shen, Biosensors and Bioelectronics, 2010, **26**, 327–332.
51 Y. Zhang, H. Jiang, X. Wang, Analytica Chimica Acta, 2015, **870**, 1–7.

Figure Captions

Fig. 1 A self–assembly method of this sensor.

Fig. 2 Square wave voltammograms measurement from –620 to –5 mV under a pulse amplitude of 25 mV and a frequency of 10 Hz, with a step potential of 4 mV in 10 mL of PBS containing 0.2 M NaCl (pH 7.0), after reacting with 0 M and 10^{-6} M Ag^{+} ion for 60 minutes and then immersing into AQDS solution containing 0.2 M NaCl for 360 minutes.

Fig.3 (A) The SEM image of NPG. (B) Cyclic voltammetry diagrams of GCE, GCE/NPG, using a 0.1 M KCl solution containing 5.0 mM ferro/ferricyanide, with potential range of –0.3 to 0.8 V, and a scan rate of 100 $mV \cdot s^{-1}$. (C) Electrochemical impedance spectra of GCE, GCE/NPG, using phosphate buffer (pH 7.4) containing 5 mM ferro/ferricyanide and 10 mM KCl, with frequency range of 0.1–10^{5} Hz, a bias potential of 0.19 V vs. SCE and an AC amplitude of 5 mV.

Fig.4 (A) SWV curves at target DNA concentrations of (a) 0 M, (b) 1×10^{-10} M, (d) 1×10^{-9} M, (d) 1×10^{-8} M, (e) 1×10^{-7} M, (f) 1×10^{-6} M, (a) to (j). **(B)** The linear relationship between peak current and common logarithm of target concentration (n = 3).

Fig. 5 The repeatability of the same biosensor for 1.0×10^{-8} M Ag^{+} (different line represents different testing sample with the same biosensor).

Fig. 6 Selectivity and interference study in the analysis of Ag^{+} by the duplex–like DNA system. The data were averages of three replicate measurements.

Table 1 Comparison with other published Ag^+ detection sensor.

method	Materials	Linear range ($mol \cdot L^{-1}$)	LOD ($mol \cdot L^{-1}$)	References
fluorescent sensor	Sybr Green I	5×10^{-8}–7×10^{-7}	3.2×10^{-8}	16
fluorescent sensor	carbon nanoparticles	5×10^{-9}–5×10^{-6}	5×10^{-9}	17
impedimetric immobilized DNA–based sensor	ordered mesoporous carbon nitride material	1×10^{-10}–1×10^{-5}	5×10^{-11}	18
Forster resonance energy transfer (FRET)	Layered molybdenum disulfide (MoS2)	1×10^{-9}–1×10^{-7}	1×10^{-9}	41
oligonucleotide–based fluorogenic probe	Sybr Green I	5×10^{-8}–7×10^{-7}	3.2×10^{-8}	42
colorimetric and ratiometric fluorescent chemosensor for the selective detection of Ag^+	Heptamethine cyanine	6×10^{-8}–5×10^{-6}	6×10^{-8}	43
colorimetric detection of Ag^+	Gold nanoparticles	—	3.3×10^{-9}	44
colorimetric method	Hemin Silver–Ion–Mediated DNAzyme	—	2.5×10^{-9}	45
impedimetric immobilized DNA–based sensor for the detection of Ag^+	Gold electrode	1×10^{-7}–8×10^{-7}	1×10^{-8}	46
fluorescent sensor	Single–Walled Carbon–Nanotube	0–1.5×10^{-7}	1×10^{-9}	47
electrochemical nanosensors	Fe_3O_4@Au nanoparticles	1.17×10^{-7}–1.77×10^{-5}	5.9×10^{-8}	48
electrochemical voltammetric sensor	Langmuir–Blodgett film	6×10^{-10}–1×10^{-6}	4×10^{-10}	49
fluorescent sensor	triphenylmethane (TPM) dye/G–quadruplex complexes	5×10^{-7}–1.3×10^{-5}	8×10^{-8}	50
fluorescent sensor	gold nanoclusters	1×10^{-8}–1.6×10^{-5}	1×10^{-8}	51
electrochemical sensor	nanoporous gold/anionic intercalator	1×10^{-10}–1×10^{-6}	4.8×10^{-11}	This work

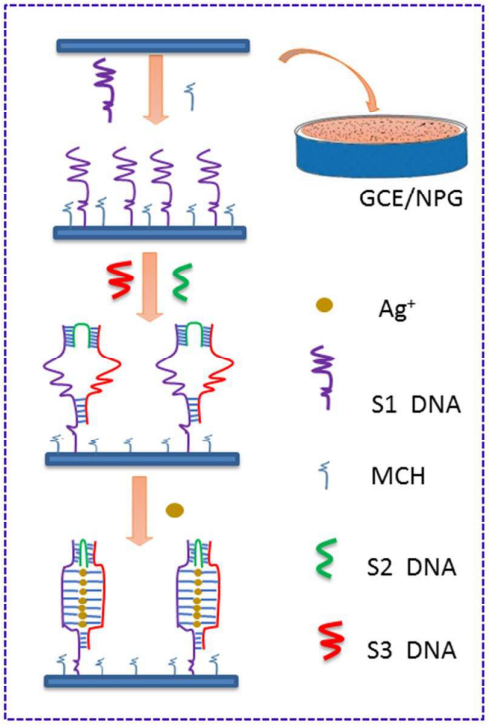

Fig.1

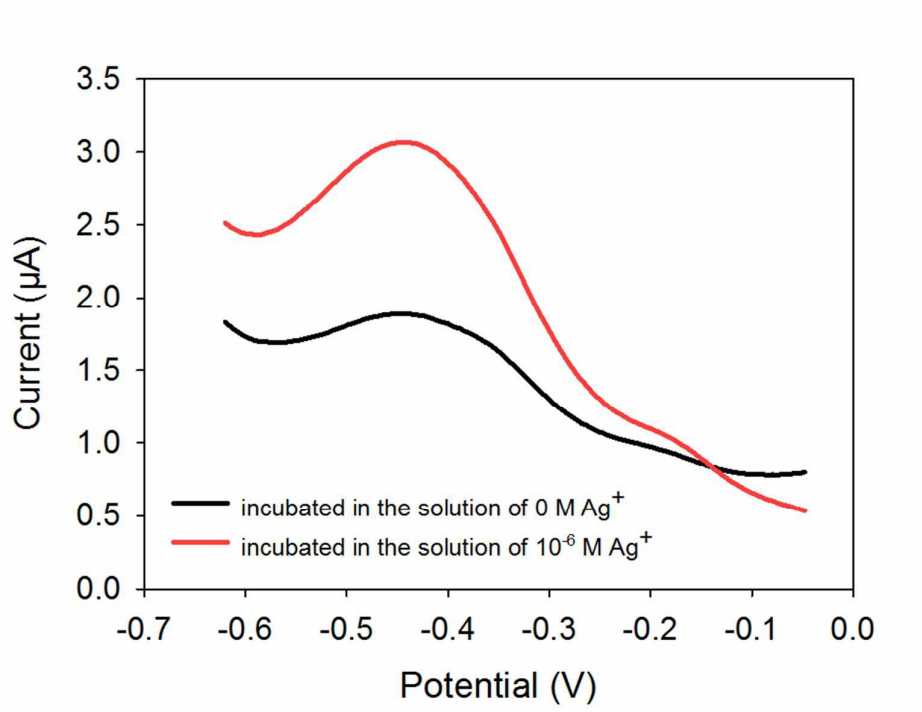

Fig. 2

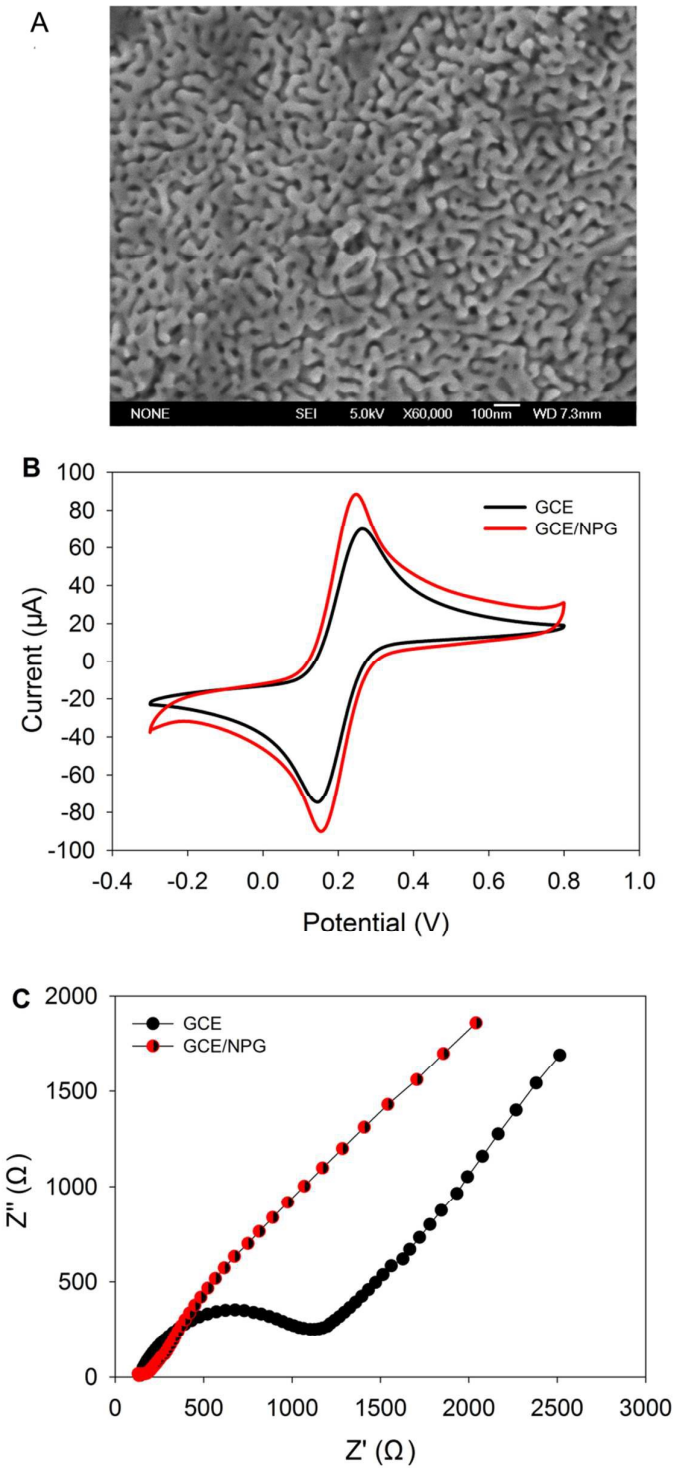

Fig. 3

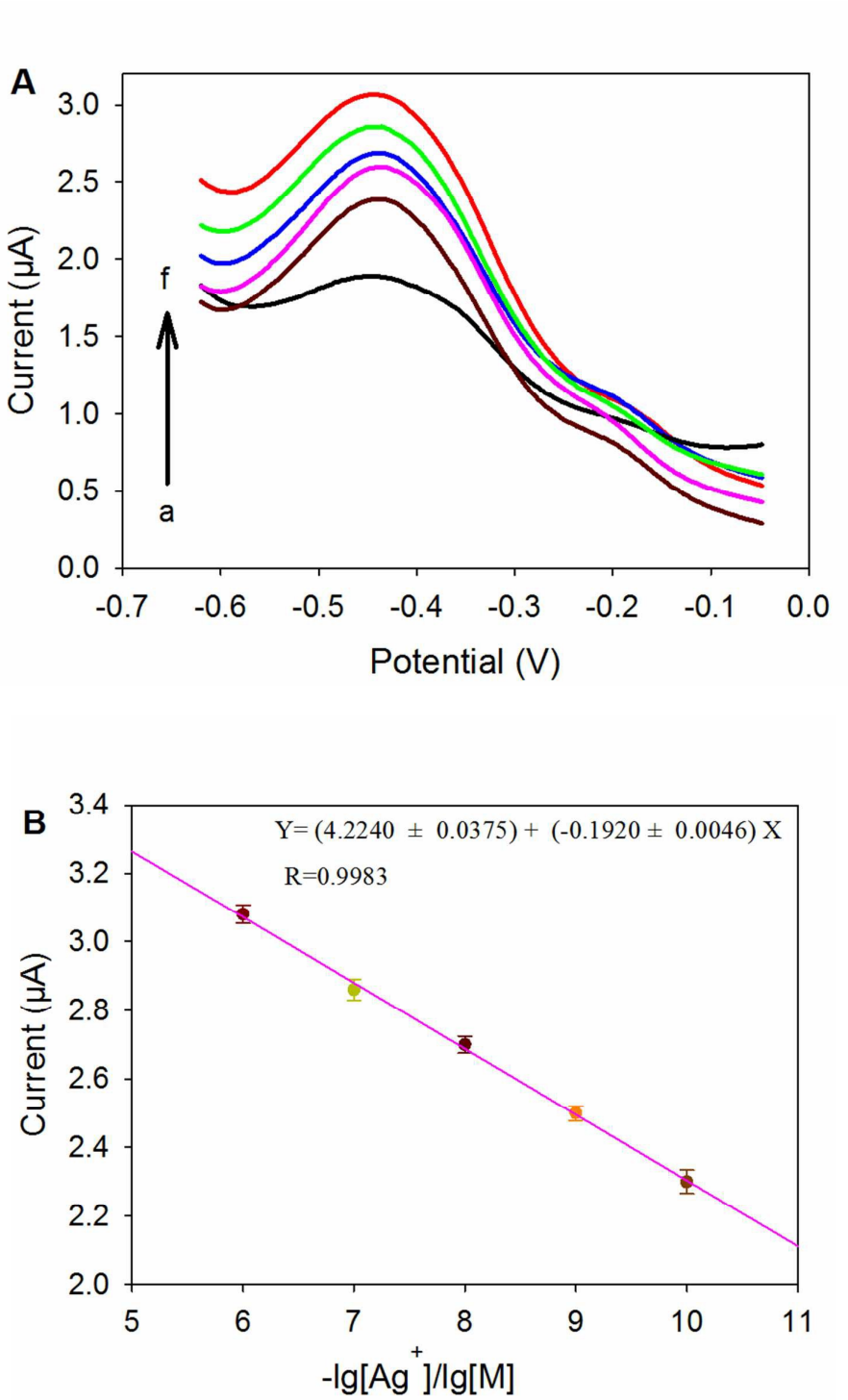

Fig. 4

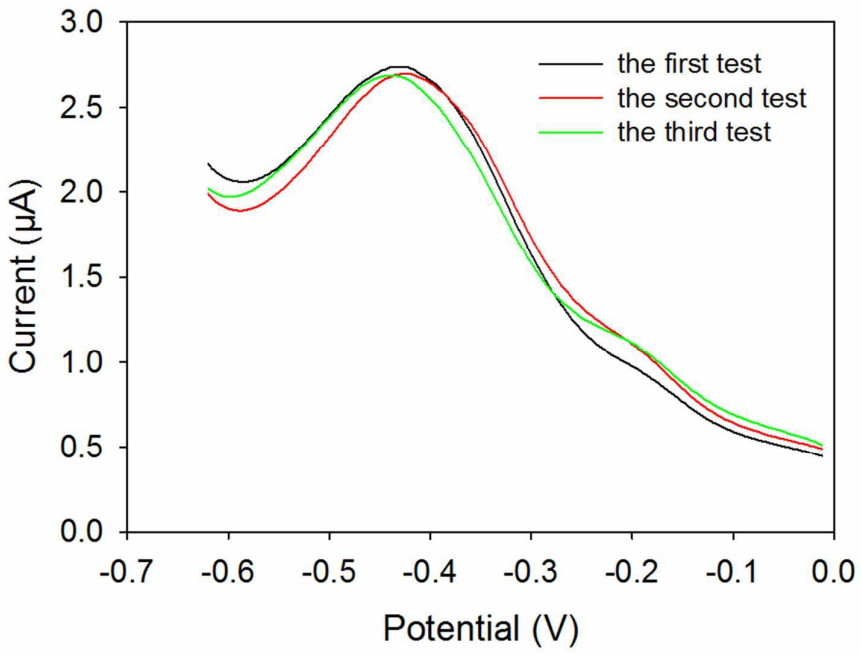

Fig. 5

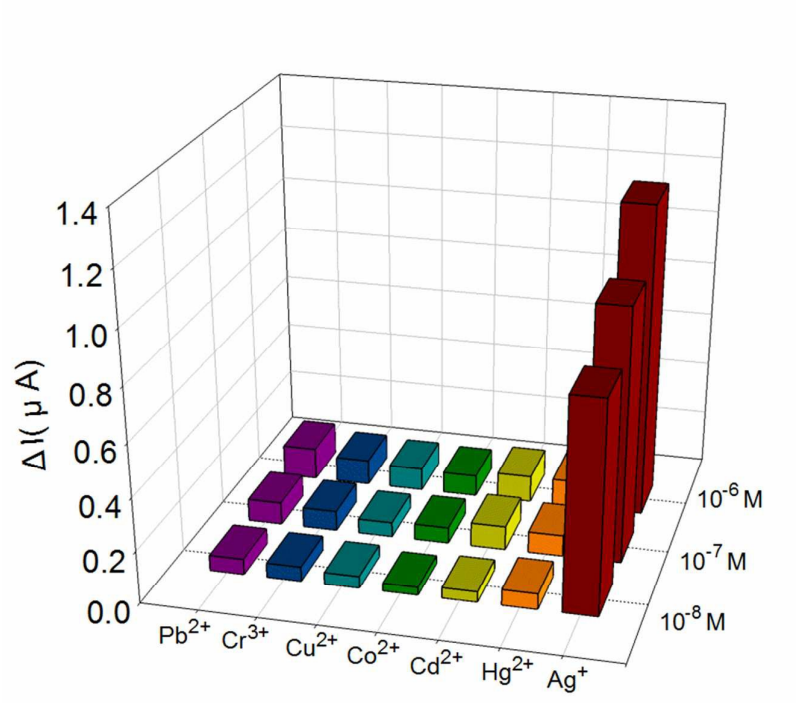

Fig. 6

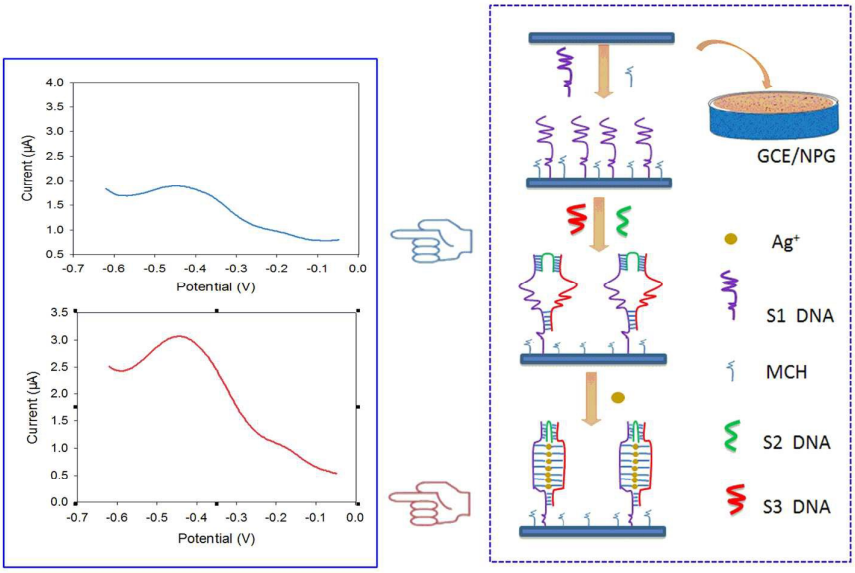

A novel biosensor for silver(I) ion detection based on nanoporous gold and duplex–like DNA scaffolds with anionic intercalator.